JOURNAL OF GEOPHYSICAL RESEARCH, VOL. 97, NO. D18, PAGES 20,751–20,769, DECEMBER 20, 1992

Three-Dimensional Simulations of Atmospheric Methyl Chloroform: Effect of an Ocean Sink

X. TIE,[1,2] C.-Y. KAO,[3] AND E. J. MROZ,[3] R. J. CICERONE,[4] F. N. ALYEA,[5] AND D. M. CUNNOLD[5]

A global three-dimensional chemical tracer model of the distribution and seasonal cycles of the surface concentration of CH_3CCl_3 is compared with surface observations from the Atmospheric Lifetime Experiment (ALE) for the years 1980-1985. Two-dimensional OH distributions calculated by a photochemical model are empirically adjusted from observed trends in the global average and the interhemispheric ratio of methyl chloroform. The effects of the recently discovered ocean sink for methyl chloroform were investigated. The model simulates the 5-year record of observations made at the five ALE sampling sites to generally within ±5% of the observed mean. The calculated average global lifetime of methyl chloroform is 5.7 ± 0.3 years. The estimated global mean OH concentration is $6.5 \pm 0.4 \times 10^5$ cm^{-3}. However, the inclusion of the ocean sink does not significantly improve the simulation of the observed interhemispheric gradient of methyl chloroform. Atmospheric transport dominates the simulated CH_3CCl_3 seasonal cycle throughout the northern hemisphere but is less important in the southern hemisphere.

1. INTRODUCTION

The global distribution of sources of greenhouse gases invites the use of general circulation models (GCMs) of the atmosphere to examine the 3-dimensional distributions, trends, and seasonal cycles of these trace gases. Although there are questions about the ability of GCMs to predict future climate, these models credibly simulate the atmospheric pressure, wind, temperature, and precipitation distributions of present-day climate [*Houghton et al.*, 1990]. They have been used to simulate the global distribution of inert trace gases such as CFC-11, which has not only a well-known, solely human source but also an extended history of atmospheric measurements for validation [*Kao et al.*, 1992; *Prather et al.*, 1987].

The global distribution of other important trace gases such as methane, the large family of nonmethane hydrocarbons, and sulfur-, halogen-, and nitrogen-bearing compounds are affected by chemical oxidation reactions that occur within the atmosphere. Knowing the global distribution of OH radicals is central to predicting the atmospheric effects of these oxidation processes. However, the global distribution of hydroxyl radical in the atmosphere is not well known. Routine measurements of OH radical concentrations that are representative of large portions of the troposphere are not yet technically feasible [*Brune*, 1992]. Previous estimates of the global tropospheric average OH concentration were inferred from observations of methyl chloroform (CH_3CCl_3), a widely used industrial solvent [*Taylor et al.*, 1991].

Methyl chloroform is atmospherically important as a significant source of stratospheric chlorine that catalytically destroys ozone in the stratosphere. It is also a minor greenhouse gas [*Ramanathan et al.*, 1987]. There are no known natural sources of CH_3CCl_3. Before the recent discovery of an apparent ocean sink for methyl chloroform [*Butler et al.*, 1991], it was thought that the sole tropospheric sink of CH_3CCl_3 was through reaction with OH radicals [*Lovelock*, 1977]. The trend in the atmospheric concentration of CH_3CCl_3 has been measured as part of the Atmospheric Lifetime Experiment (ALE) at five locations (Figure 1) since 1978 [*Prinn et al.*, 1987]. Because the flux of CH_3CCl_3 to the troposphere can be closely approximated by industrial production figures and its destruction through reaction with OH can be expressed as simple bimolecular reaction rate, the global distribution, seasonal cycle, and trend of CH_3CCl_3 have been used to elucidate the global distribution, seasonal cycle, and trend of atmospheric OH.

Recently, chemical tracer models (CTMs) based upon GCMs have been used to examine the three-dimensional global distribution of CH_3CCl_3. *Spivakovsky et al.* [1990] and *Taylor et al.* [1991] simulated CH_3CCl_3 using OH fields generated by their two-dimensional and three-dimensional models. Both groups found that their photochemical models coupled with three-dimensional CTMs underpredicted the observed concentration and trend in atmospheric CH_3CCl_3. Spivakovsky et al. concluded that their photochemical model overpredicted OH because of inadequate treatment of OH losses through reactions with nonmethane hydrocarbons. Taylor et al. concluded that the flux of CH_3CCl_3 to the atmosphere is somewhat larger than estimated by *Prinn et al.* [1987].

In this paper, we address this issue with a three-dimensional chemical tracer model based upon the Los Alamos GCM and a two-dimensional photochemical model of tropospheric OH. We simulate the global distribution, trend, and seasonal cycle of CH_3CCl_3 from 1980 to 1985. The results are compared with the ALE record for the same time period. We explore whether the interhemispheric OH concentration ratio can be constrained by the ALE observations in the two hemispheres. We then examine the effects of the recently reported ocean sink for CH_3CCl_3 [*Butler et al.*, 1991].

In section 2 we briefly describe the model configuration. In section 3 we describe four different 5-year simulations of the concentrations of CH_3CCl_3 and compare them to the observations of the ALE network. In section 4 we analyze the effects of atmospheric transport and the inferred OH distribution on the seasonal cycles of CH_3CCl_3.

[1]Scripps Institution of Oceanography, University of California at San Diego, La Jolla.
[2]Now at National Center for Atmospheric Research, Boulder, Colorado.
[3]Los Alamos National Laboratory, Los Alamos, New Mexico.
[4]University of California at Irvine, Irvine.
[5]Georgia Institute of Technology, Atlanta.

Paper number 92JD02085.
0148-0227/92/92JD-02085 $05.00

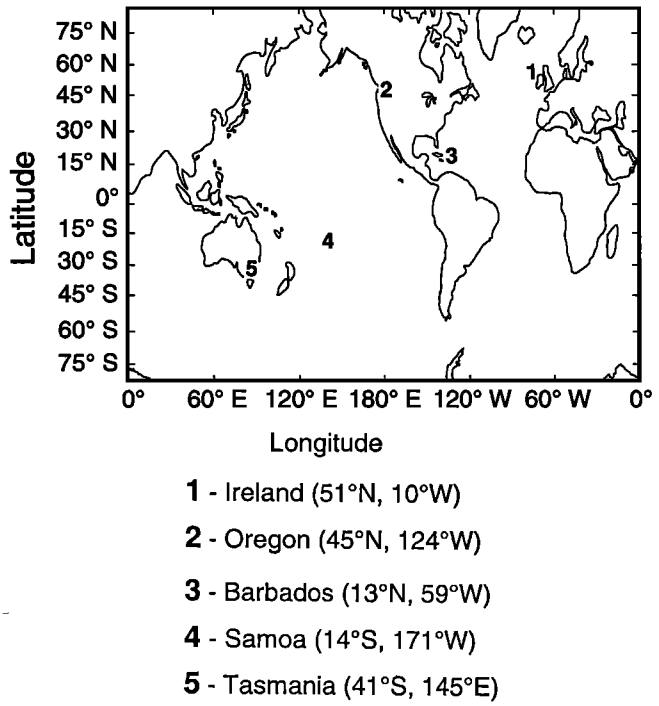

Fig. 1. Geographical locations of the ALE observation sites.

2. Model Configuration

The Los Alamos CTM is a grid point model that uses dynamical and thermodynamical input from the Los Alamos GCM [*Malone et al.*, 1986] to simulate the global atmospheric transport of chemical species. There are 40 latitudinal grid points with a 4.5° interval and 48 longitudinal grid points with a 7.5° interval. In the vertical dimension, the model has 20 levels in the sigma coordinate system. The model top is at about 9 mbar (30 km). Table 1 shows the heights and spacings of the vertical levels.

Model transport includes horizontal advection, convection, horizontal diffusion, and vertical diffusion. Five precalculated dynamical and thermodynamical variables are required: the horizontal winds (u and v), the vertical wind (w), temperature (T), and the vertical diffusion coefficient (K). These variables are calculated once each model-day by the Los Alamos GCM and are linearly interpolated in 30-min time steps for the simulations of CH_3CCl_3. Details of the model transport scheme can be found in the work of *Kao et al.* [1992].

There are several key differences between this model and those used by *Spivakovsky et al.* [1990] and *Taylor et al.* [1991]. This model has 20 vertical levels rather than the nine vertical levels used by Spivakovsky et al. and the seven levels used by Taylor et al. Our horizontal resolution is 4.5° latitude × 7.5° longitude as compared with 8° × 10° [Spivakovsky et al.] and 2.5° × 2.5° [Taylor et al.]. Taylor et al. used analyzed wind fields from the European Center for Medium Range Weather Forecasting, whereas both we and Spivakovsky et al. used wind fields generated by a parent GCM. A final significant difference is that Taylor et al. used a Lagrangian transport scheme, whereas both we and Spivakovsky et al. use an Eulerian grid point scheme.

TABLE 1. Vertical Levels of the Los Alamos GCM

Level	z, km	P, mbar	T, °K	Density ×10^{17}/cm^3
20	30.9	8.9	232	2.8
19	27.9	13.8	224	4.5
18	25.6	19.7	225	6.4
17	23.0	29.6	222	9.7
16	20.3	45.4	219	15.0
15	17.9	67.1	215	22.6
14	15.6	99.7	209	34.5
13	13.2	149	210	51.4
12	11.1	211.2	214	71.4
11	9.2	282.2	221	92.5
10	7.7	352.3	230	111.0
9	6.5	423.3	238	129.0
8	5.4	493.4	245	146.0
7	4.4	563.4	252	162.0
6	3.5	634.5	258	178.0
5	2.7	704.5	264	193.0
4	2.0	775.6	267	210.0
3	1.3	845.6	274	224.0
2	0.6	916.7	280	237.0
1	0.0	982.8	285	250.0

Distribution of Sources

Total annual industrial emissions of CH_3CCl_3 for 1978 through 1985, as estimated by *Prinn et al.* [1987] and updated by *Midgley* [1989], are listed in Table 2. *Taylor et al.* [1991] concluded that the available measurements of CH_3CCl_3 from 1982 to 1984 were better explained by emission estimates closer to those of Midgley. For this study, we used Midgley's estimates. However, estimates of emissions from eastern Europe, the former USSR, and China are not included. Elevated concentrations of methyl chloroform have been measured in China, suggesting that it may be a significant source region [*Rasmussen et al.*, 1982]. The inability to estimate the source strength of the former USSR, eastern Europe, and China will result in an unknown but probably small underestimation of the CH_3CCl_3 concentration measured at the ALE sites.

Although the global annual emission rate of CH_3CCl_3 can be approximated from industry-supplied annual production figures, the spatial and seasonal distribution of the emissions are unknown. We globally distribute CH_3CCl_3 emission sources in the same manner as used by *Spivakovsky et al.* [1990]. Documented electrical power consumption in individual countries is taken to be an index of technological advancement that can be used to apportion CH_3CCl_3 use and, consequently, emissions. This method has been used successfully to simulate CFC-11 and CFC-12 [*Prather et al.*, 1987]. For CH_3CCl_3, the annual release from each grid square was computed as the product of the total annual release of CH_3CCl_3 (as shown in Table 2) and the fractional annual release of CFC-11 from each grid as estimated by Spivakovsky et al. We assumed that the annual emissions were uniformly released throughout the year. The emissions were released into the two lowest vertical levels of the model because the first 1 km of the planetary boundary layer is rapidly mixed vertically.

TABLE 2. Annual Average Source Strength of CH_3CCl_3 in the Model

Year	CH_3CCl_3, [a] × 10^6 g/year	CH_3CCl_3, [b] × 10^6 g/year
1978	476.2	524.0
1979	540.6	506.0
1980	544.9	552.0
1981	538.7	548.0
1982	510.9	514.5
1983	516.0	542.5
1984	550.0	600.0
1985	581.2	590.0

[a] Prinn et al. [1987].
[b] Midgley [1989].

The Chemical Sink of CH_3CCl_3

The sole chemical reaction within the troposphere that destroys methyl chloroform is the reaction with OH radicals. Photolysis by UV is an additional loss mechanism that occurs in the stratosphere. In our model these processes are expressed as

$$CH_3CCl_3 + OH \rightarrow \text{product with a reaction rate of } k_1$$

$$CH_3CCl_3 + h\nu \rightarrow \text{product with a photolysis rate of } J_1$$

The photolysis rate J_1 is calculated using the technique employed by *Prinn et al.* [1975]. Reaction rate k_1 is 5.0×10^{-12} exp(-1800/T) [*DeMore et al.*, 1990]. Following the completion of this work, it was reported that this reaction rate should be revised downward [*Talkudar et al.*, 1992]. The effect of this revision is discussed below.

Model Initialization

The initial two-dimensional (latitude-altitude) distribution of CH_3CCl_3, corresponding to the monthly mean values of July 1978, was constructed from ALE surface measurements and measured vertical profiles [*Khalil and Rasmussen*, 1984; *Knapska et al.*, 1985; *Rasmussen and Khalil*, 1983].

Methodology for Estimating the Global OH Field

We began with monthly average two-dimensional OH distributions as calculated from a two-dimensional photochemical model [*Tie et al.*, 1991]. Figure 2 shows the initial OH distribution in January and July. The model computes a global tropospheric mean OH concentration of 6.5×10^5 molecules/cm^{-3}. This is consistent with the range of reported values (3 to 10×10^5 molecules/cm^{-3}) as reviewed by *Taylor et al.* [1991]. The distributions show that OH has maximum at 20°S and 700 mbar in January and at 20°N and 700 mbar in July. This model computes the interhemispheric OH concentration ratio ($[OH]_N/[OH]_S$) to be about 0.8. This distribution, and the hemispheric asymmetry of the OH field, are similar to those found by others [*Brasseur et al.*, 1990; *Chameides and Tan*, 1981; *Taylor et al.*, 1991]. Figure 3 shows the tropospheric seasonal cycle of OH. The amplitude of the seasonal cycle of OH in the northern hemisphere is somewhat smaller than that in the southern hemisphere because of the higher concentrations of CH_4, CO, and nonmethane hydrocarbons in the northern hemisphere. *Spivakovsky et al.* [1990] calculated a higher OH concentration in the northern than in the southern hemisphere. They attribute this

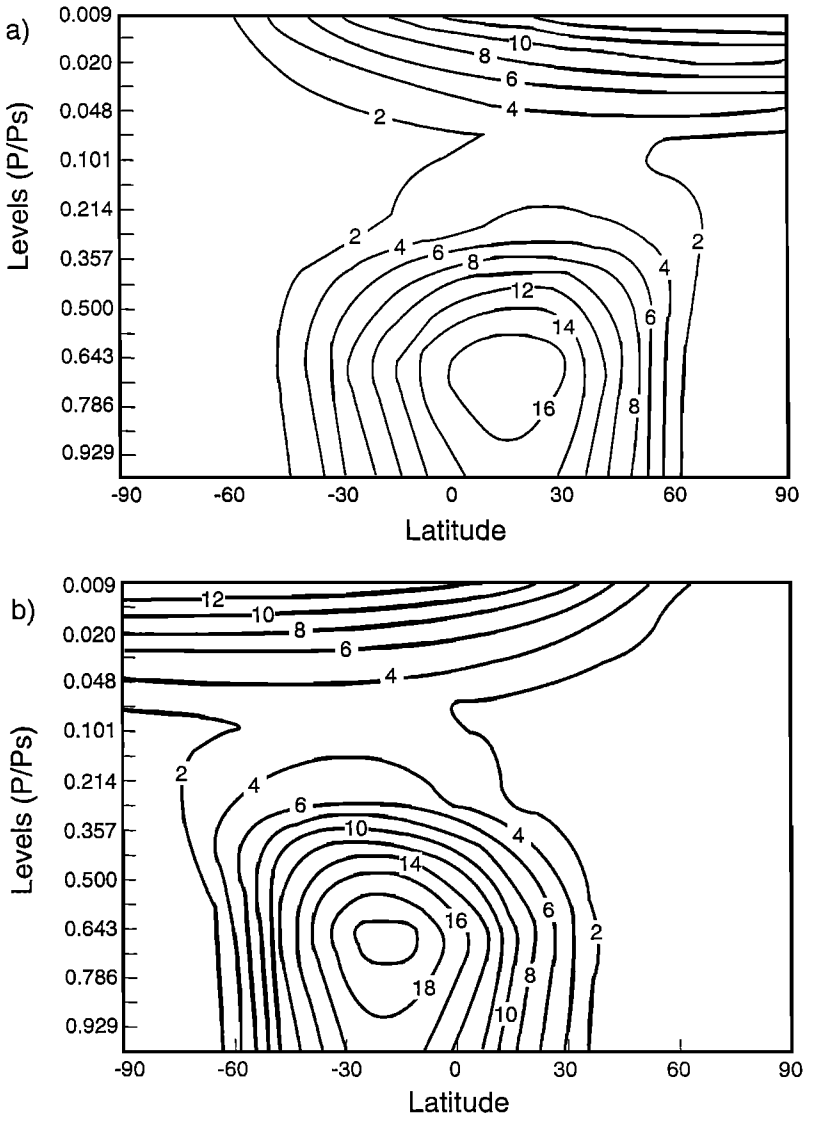

Fig. 2. Calculated initial two-dimensional OH concentration (10^5 molecules cm^{-3}) distributions for (*a*) July and (*b*) January.

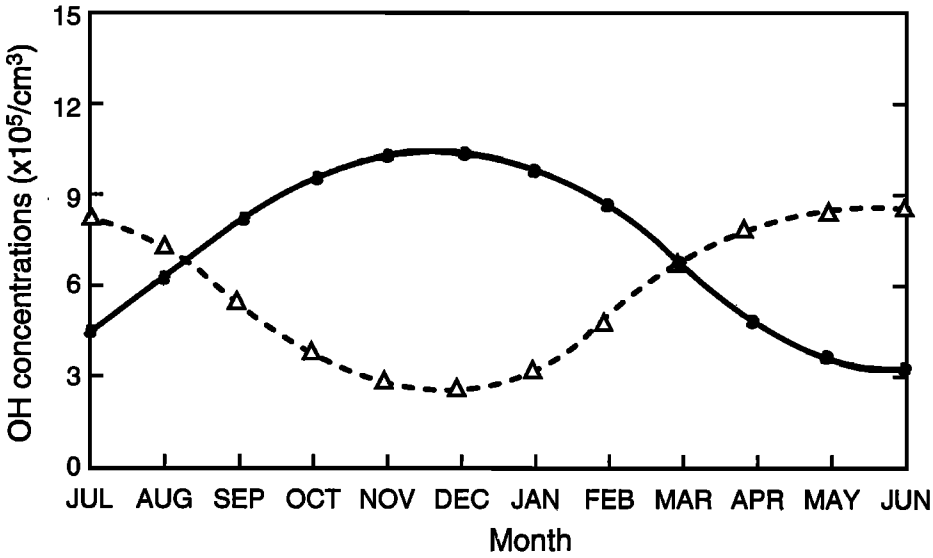

Fig. 3. Calculated initial hemispheric monthly average OH concentration ($\times 10^5$ molecules cm^{-3}) for the northern (dashed line) and southern (solid line) hemispheres.

to the higher surface albedo and the enhanced levels of NO_y and O_3 over land compared to those over the ocean.

Zonally extending the two-dimensional OH field longitudinally throughout the three-dimensional transport model is justified because the atmospheric lifetime of CH_3CCl_3 is much longer (years) than the time constant for circumzonal transport (weeks). On average, any given molecule of CH_3CCl_3 will circumnavigate the globe several hundred times before being destroyed by reaction with OH. The expected difference in OH concentrations over oceans and continents is not large enough to induce significant meridional variations in the CH_3CCl_3 distribution. For all of the simulations discussed below, we assumed that there was no temporal trend in OH during the 7-year simulation.

3. Simulations of CH_3CCl_3 in the Atmosphere

Case 1: Base Case

Our base case simulation used the OH distribution derived from the two-dimensional model described above. Table 3*a* summarizes the salient features of the simulation. The lifetime of CH_3CCl_3 in the model is 6 years and the interhemispheric transport time constant is 6 months. This lifetime is consistent with the results of other studies [*Prinn et al.*, 1987; *Spivakovsky et al.*, 1990; *Taylor et al.*, 1991]. The interhemispheric time constant is somewhat shorter than the 7- to 12-month range found to give acceptable simulations for CFC-11 [*Prather et al.*, 1987]. We have found that this model, with a 6-month interhemispheric transport time constant, accurately simulates the interhemispheric gradient of CFC-11 [*Kao et al.*, 1992].

Figure 4 shows the calculated surface distribution of CH_3CCl_3 averaged for January and July from 1980 to 1985. Longitudinal concentration gradients associated with sources of CH_3CCl_3 in the industrialized regions of the northern hemisphere are apparent. These features are absent in the southern hemisphere because of the absence of major sources there.

Figure 5 shows the calculated meridional cross section of CH_3CCl_3 also averaged for January and July from 1980 to 1985. The distribution is consistent with the majority of CH_3CCl_3 being released at the surface in the northern hemisphere and mixing rapidly vertically throughout the northern troposphere. A tongue of the 105-ppt contour extends from the northern to southern hemisphere. The northern upward branch of the Hadley cell delivers CH_3CCl_3–laden air from the source region of the northern mid-latitudes to the upper troposphere of the southern hemisphere. The slightly positive vertical gradients of CH_3CCl_3 in the southern hemisphere are a manifestation of upper tropospheric transport from the northern to the southern hemisphere. This feature has been observed in vertical profile measurements taken in the southern hemisphere [*Fraser et al.*, 1986]. The concentration of CH_3CCl_3 drops sharply in the stratosphere, where it is destroyed by photolysis.

Figure 6 shows the monthly averaged CH_3CCl_3 concentrations measured at the ALE sites together with results of the model simulation from July 1980 through June 1985. Table 3*b* compares the results of the simulation for each of the ALE sites. We assess

TABLE 3*a*. Features of Four Model Simulations Comparing Modeled and Measured Concentrations of CH_3CCl_3 at the ALE Sampling Locations

Case	$[OH]_G$	$[OH]_N$, $\times 10^5$ cm^{-3}	$[OH]_S$	Lifetime, years	N-S, [a] kt	N-S Flux, [b] t/year	$\tau_{N\text{-}S}$, [c] months
1	6.5	5.8	7.2	6.4	134	267	6
2	8.2	7.4	9.1	5.4	134	267	6
3	8.2	5.2	11.3	5.5	148	312	5.7
4	6.5	5.8	7.2	5.7	138	274	6

[a] Burden difference of CH_3CCl_3 in northern and southern hemispheres.
[b] Annual average interhemispheric transport of CH_3CCl_3.
[c] Interhemispheric transport time constant.

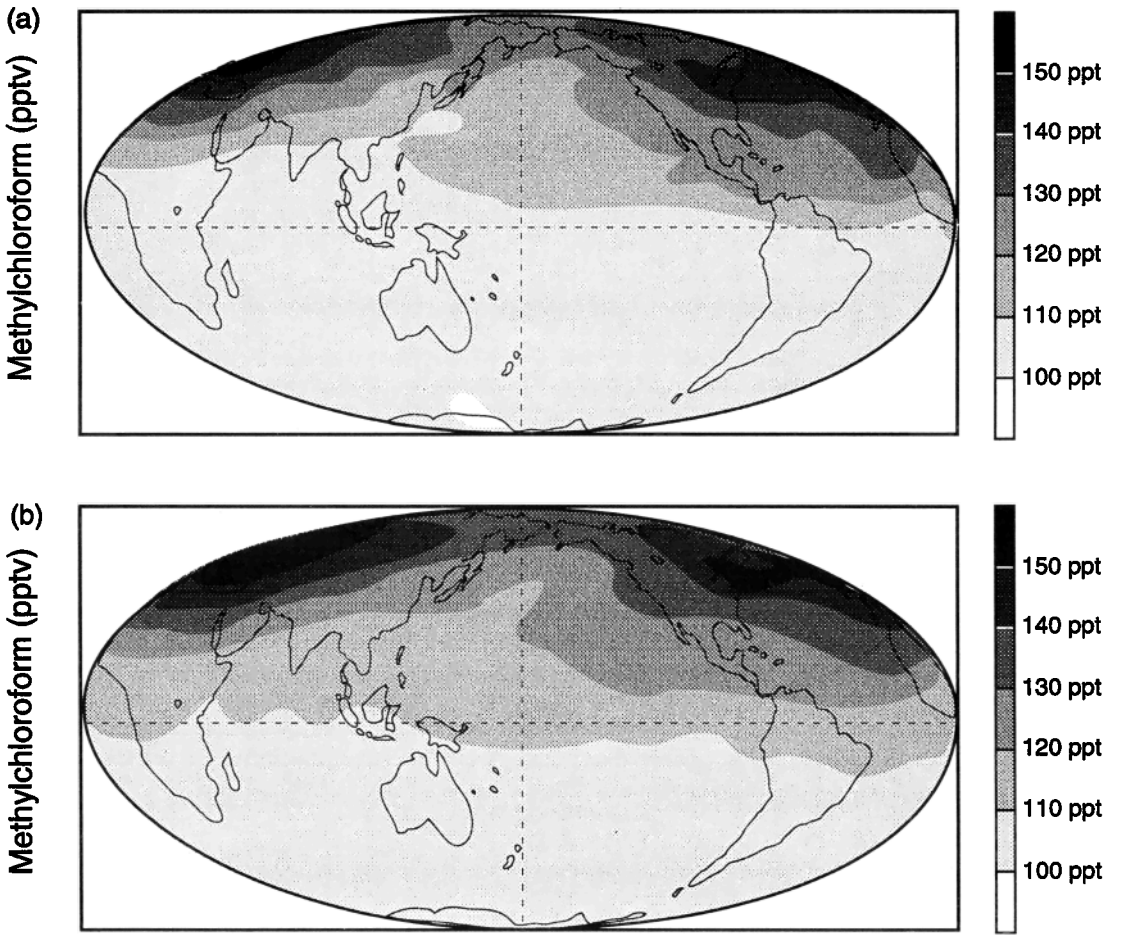

Fig. 4. Calculated (case 3; see text) mean surface CH_3CCl_3 concentration (parts per thousand) for (*a*) January and (*b*) July from 1980 to 1985.

model bias and some of the uncertainty associated with these simulations by reporting both the mean and the standard error of the difference between the observed monthly average methyl chloroform concentration and the simulated value for each of the five ALE sites. It is apparent that this simulation systematically overestimates CH_3CCl_3 at all five ALE sites because model bias values in Table 3*b* are positive for all sites. Furthermore, the standard error of the mean model bias is small compared to the bias for all sites except Cape Meares, Oregon. This suggests that the OH concentration fields are generally too low. The relatively good agreement found at Cape Meares, Oregon, is believed to be fortuitous. In an earlier study we showed that this model consistently underestimates CFC-11 by about 7 to 12 ppt at Cape Meares [*Kao et al.*, 1992]. We attributed this underestimation to the model's inability to capture regional scale circulation features that appear to be influencing the CFC-11 observations at the Cape Meares sampling location. Therefore we expect that a good simulation of methyl chloroform would underestimate CH_3CCl_3 at Cape Meares by an approximately proportional amount of about 5 to 8 ppt. The ~30-ppt interhemispheric gradient is underpredicted by 5.8 ± 1.3 ppt.

Case 2: Observationally Constrained Global OH

We concluded from our base case, case 1, that the two-dimensional photochemical model globally underestimates the OH concentrations. We elected to constrain the two-dimensional monthly average OH concentration grid by the global average OH calculated from the observed trend of CH_3CCl_3 at the ALE sites. One advantage of this approach is that global OH is constrained by the ALE observations themselves. Secondly, the effects of the recently discovered ocean sink for CH_3CCl_3 [*Butler et al.*, 1991] are also implicitly incorporated into this empirical estimate of the global and annual mean OH concentration.

A simple equation balances the increasing emission rate and concentration of CH_3CCl_3 with its chemical destruction by reaction with OH:

$$\Delta[CH_3CCl_3]_G/\Delta t = E_G - k_1[OH]_G[CH_3CCl_3]_G \quad (1)$$

where $\Delta[CH_3CCl_3]_G/\Delta t$ is the annual increase in the global average concentration of CH_3CCl_3; E_G is the annual increase in the global emissions of CH_3CCl_3; and $k_1[OH]_G[CH_3CCl_3]_G$ is the rate expression for the globally averaged chemical loss of CH_3CCl_3 reaction with OH. The value of k_1 is temperature-dependent. We used the pressure-weighted average temperature of the model troposphere. Solving the equation for $[OH]_G$, we get

$$[OH]_G = (\Delta[CH_3CCl_3]_G/\Delta t - E_G)/-k_1[CH_3CCl_3]_G$$

In Table 4 we present the annual average $[OH]_G$ for the period 1980 to 1983 when observations are available from all five ALE sites for the entire period. For the entire period, the average $[OH]_G$ is $8.2 \pm 0.2 \times 10^5$ cm^{-3}, which is about 25% higher than the value used in the case 1 simulation discussed above. This value is, nevertheless, still within the range of $7.7 \pm 1.4 \times 10^5$ cm^{-3}

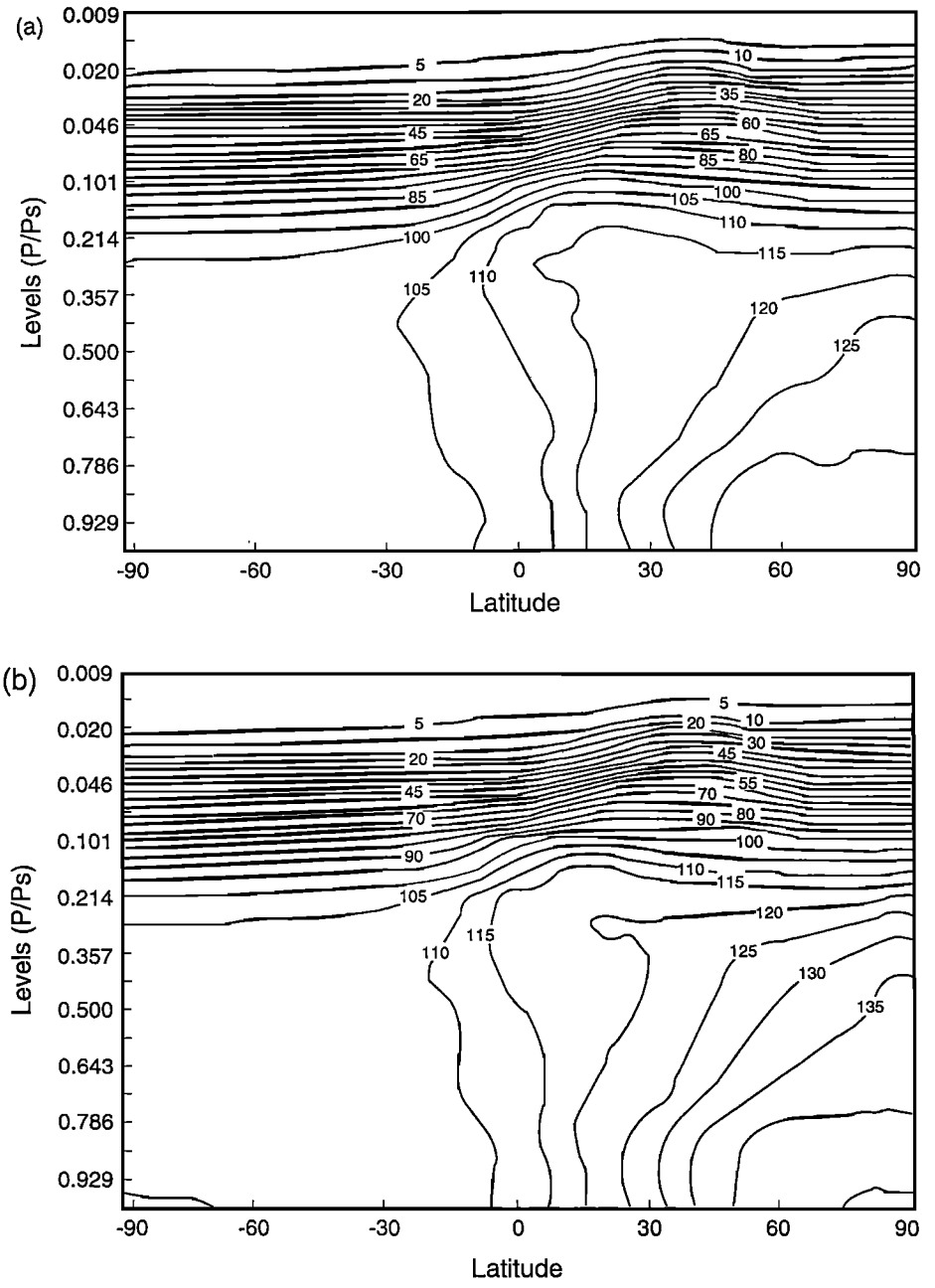

Fig. 5. Calculated (case 3; see text) zonal mean CH_3CCl_3 concentration (parts per thousand) for (*a*) January and (*b*) July from 1980 to 1985.

cited by *Prinn et al.* [1987] and close to the values (6 to 8 × 10^5 cm^{-3}) used by *Spivakovsky et al.* [1990].

By this approach we constrain the global average OH by the relationships discussed above and test the accuracy of the monthly averaged relative meridional and vertical distributions of OH predicted by the two-dimensional photochemical model.

For case 2, then, we uniformly increased the monthly average OH concentrations within each grid cell as used in case 1 by 25%. The interhemispheric ratio is unchanged from that in case 1. Figure 7 compares the observations with the simulation at the five ALE sites. The results are presented as the mean model biases and associated standard error of the mean model biases for each of the five ALE sites in Table 3*b*. We find that the positive model biases found for Case 1 are now negative at all locations except for Adrigole, Ireland. The interhemispheric gradient of ~30 ppt remains underpredicted by ~5.8 ppt. The mean model biases are all significant at the 95% confidence level, which is to say that there is a <5% chance that the null hypothesis, which is that the model bias is zero, is true.

We see that case 2 is improved over case 1 inasmuch as, for three (Ireland, Samoa, and Tasmania) of the five ALE locations, the absolute value of the mean bias was reduced from that in case 1. The model biases for Oregon and Barbados were substantially degraded. Increasing the global mean OH reduces the atmospheric lifetime of methyl chloroform to 5.4 years, which is just within the accepted limits of 6.3 (+1.2, -0.9) years [*Prinn et al.*, 1987]. We conclude that scaling the OH concentration grid to the global trends in methyl chloroform emissions and concentrations improves the accuracy of the simulation. However, agreement, in a statistical sense, with the observations is not satisfactory.

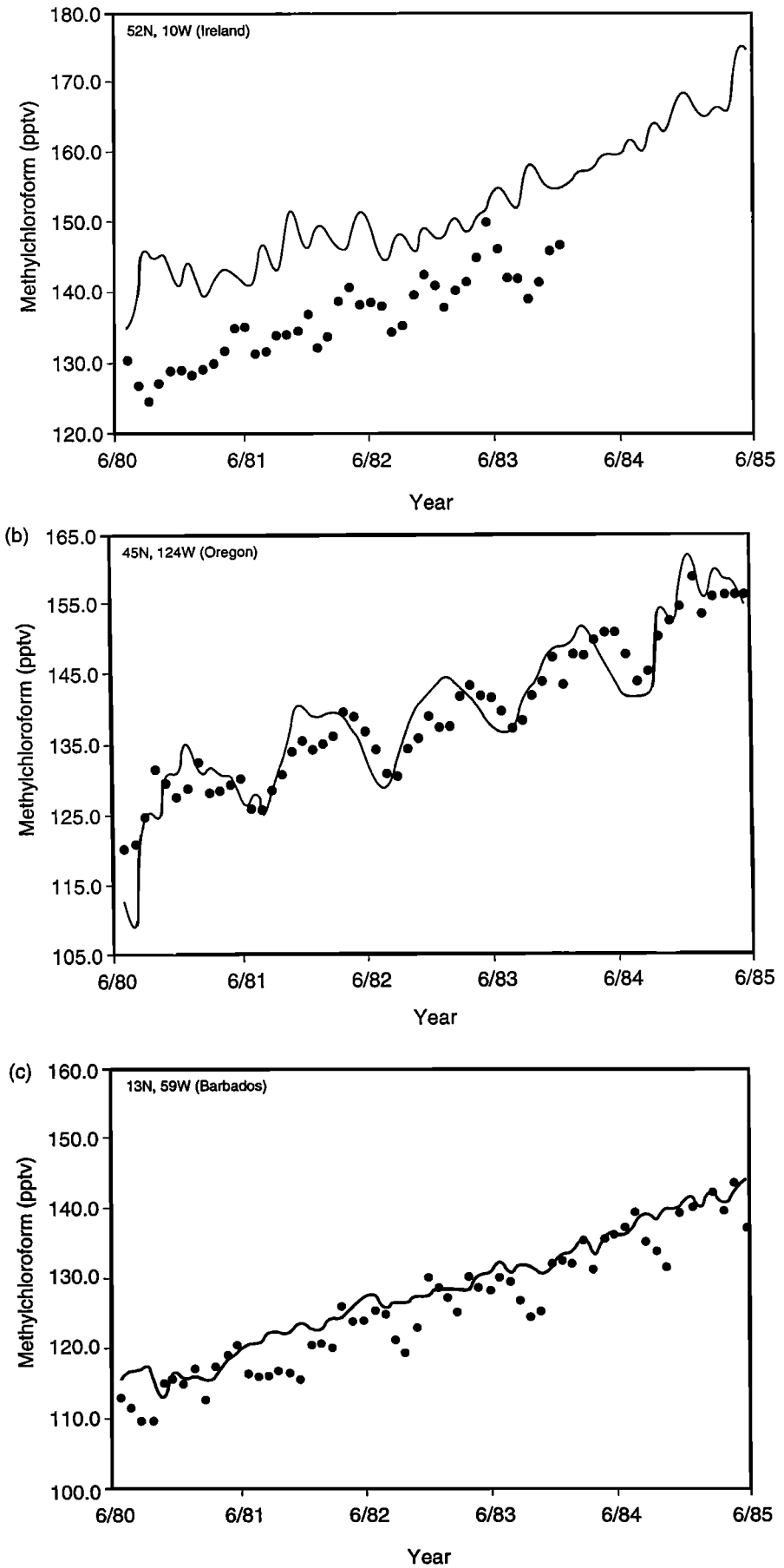

Fig. 6. Case 1. Modeled (solid line) and measured (dotted line) surface concentration of CH_3CCl_3 for the five ALE sites (*a*) Adrigole, Ireland, (*b*) Cape Meares, Oregon, (*c*) Ragged Point, Barbados, (*d*) American Samoa, and (*e*) Cape Grim, Tasmania.

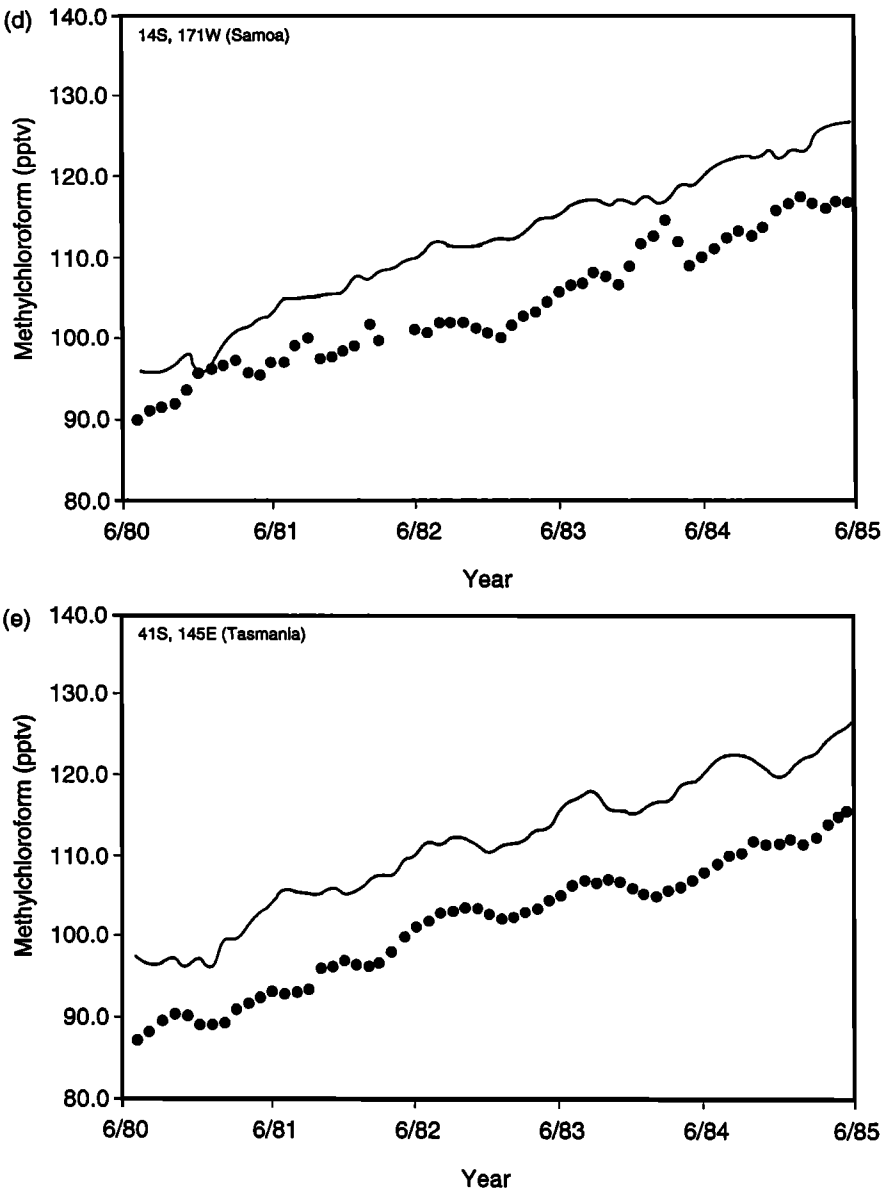

Fig. 6. (continued)

Case 3: Constraint of the Interhemispheric OH Ratio

We now explore whether the ALE data record combined with three-dimensional simulations of methyl chloroform can help constrain the interhemispheric OH concentration ratio. Equation (1) can be modified to describe the rate of change of the mean concentration of methyl chloroform in each hemisphere:

$$\Delta[CH_3CCl_3]_N/\Delta t = E_N - TNS - k_1[OH]_N[CH_3CCl_3]_N \quad (2a)$$

and

$$\Delta[CH_3CCl_3]_S/\Delta t = E_S + TNS - k_1[OH]_S[CH_3CCl_3]_S \quad (2b)$$

where TNS is the average mass of methyl chloroform annually transported from the northern to southern hemisphere. Solving each equation for [OH] and dividing (2*a*) by (2*b*) results in an approximate solution for $[OH]_N/[OH]_S$.

It is an approximate solution for the following reasons:

1. The value of TNS is sensitive to the interhemispheric transport time constant of the model. For both CFC-11 [*Kao et al.*, 1992] and methyl chloroform (case 2), this model gives an interhemispheric time constant of approximately 6 months. Other three-dimensional models have indicated a range of values from 7 to 13 months. These differences result from differences among the models. For example, our model resolves the troposphere into 13 levels below 150 mbar compared with seven layers in the model of *Spivakovsky et al.* [1990]. This difference is important because interhemispheric transport takes place primarily in the upper tropical troposphere. Differences in the speed of vertical diffusion and transport between layers could affect the interhemispheric transport time constant because most of the interhemispheric transport takes place in the upper tropical troposphere (c.f. Figure 5).

Furthermore, the term TNS is itself sensitive to $[OH]_N/[OH]_S$. Note that we calculated TNS using the value of 267 Tg/year, as calculated for case 2. When TNS was calculated from the results of case 3, the value increased to 312 Tg/year. To constrain $[OH]_N/[OH]_S$ further will require an iterative approach that would converge on the optimal value for TNS.

2. The term describing the growth rate of the northern hemis-

TABLE 3*b*. Summary of Model Biases for Each Case

	IRE,[a] ppt	ORE,[a] ppt	BAR,[a] ppt	SAM,[a] ppt	TAS,[a] ppt	NH,[b] ppt	SH,[c] ppt	Global,[d] ppt	N-S,[e] ppt
Case 1									
80-81	12.3	-1.7	1.6	4.1	8.3	4.1	6.2	4.9	-2.1
81-82	12.2	0.8	3.9	7.9	10.3	5.6	9.1	7.0	-3.5
82-83	8.3	0.9	2.0	10.6	9.3	3.7	9.9	6.2	-6.2
83-84		0.4	2.2	8.2	11.4	1.3	9.8	5.6	-8.5
84-85		0.9	2.0	9.0	11.3	1.5	10.2	5.8	-8.7
Mean	10.9	0.3	2.3	8.0	10.1	3.2	9.0	5.9	-5.8
SEM[f]	±1.3	±0.5	±0.4	±1.1	±0.6	±0.8	±0.7	±0.3	±1.3
Case 2									
80-81	5.4	-8.5	-5.2	-2.7	1.5	-2.8	-0.6	-1.9	-2.2
81-82	3.2	-8.0	-5.0	-1.1	1.3	-3.3	0.1	-1.9	-3.4
82-83	-2.7	-10.0	-8.9	-0.3	-1.5	-7.2	-0.9	-4.7	-6.3
83-84		-12.2	-10.4	-4.4	-1.4	-11.3	-2.9	-7.1	-8.4
84-85		-13.4	-12.3	-5.2	-3.0	-12.8	-4.1	-8.5	-8.7
Mean	2.0	-10.4	-8.4	-2.7	-0.6	-7.5	-1.7	-4.8	-5.8
SEM[f]	±2.4	±1.0	±1.4	±0.9	±0.9	±2.0	±0.8	±1.3	±1.3
Case 3									
80-81	7.6	-6.3	-3.2	-2.6	1.2	-0.6	-0.7	-0.7	0.1
81-82	5.8	-5.5	-2.6	-0.7	1.3	-0.8	0.3	-0.3	-1.1
82-83	0.2	-7.1	-6.3	0.4	-1.4	-4.4	-0.5	-2.8	-3.9
83-84		-9.1	-7.5	-3.6	-0.9	-8.3	-2.3	-5.3	-6.0
84-85		-10.1	-9.1	-4.3	-2.5	-9.6	-3.4	-6.5	-6.2
Mean	4.5	-7.6	-5.7	-2.2	-0.5	-4.7	-1.3	-3.1	-3.4
SEM[f]	±2.2	±0.9	±1.2	±0.9	±0.7	±1.9	±0.7	±1.2	±1.3
Case 4									
80-81	7.9	-6.0	-2.7	-0.3	3.8	-0.3	1.8	0.8	-2.1
81-82	6.5	-4.9	-1.7	2.1	4.4	0.0	3.3	1.7	-3.3
82-83	1.2	-6.2	-5.0	3.5	2.1	-3.3	2.8	-0.3	-6.1
83-84		-7.9	-6.0	-0.2	2.9	-7.0	1.4	-2.8	-8.4
84-85		-8.7	-7.4	-0.5	1.6	-8.0	0.6	-1.0	-8.6
Mean	5.2	-6.7	-4.6	0.9	3.0	-3.7	1.9	-1.1	-5.7
SEM[f]	±2.0	±0.7	±1.0	±0.8	±0.5	±1.7	±0.5	±1.0	±1.3

[a] Modeled minus measured annual average concentration for indicated site.
[b] Modeled minus measured annual average concentrations for sites in the northern hemisphere; namely, Adrigole, Ireland; Cape Meares, Oregon; and Ragged Point, Barbados.
[c] Modeled minus measured annual average concentrations for sites in the southern hemisphere; namely, Point Matatula, Samoa, and Cape Grim, Tasmania.
[d] Modeled minus measured annual average concentrations for all sites.
[e] Modeled minus measured annual average concentration difference between northern and southern hemisphere sites.
[f] Standard error of the mean.

pheric mean methyl chloroform concentration, $\Delta[CH_3CCl_3]_N/\Delta t$, has an unknown accuracy because of the proximity of the three northern ALE sites to the sources and the effects of regional circulation. This appears to be less of a problem in the southern hemisphere because the two ALE sites at Samoa and Tasmania obtain very similar values for the annual mean concentration of methyl chloroform. As the observational record increases, the interhemispheric difference in methyl chloroform growth rates will become more precisely known.

3. *Midgley* [1989] estimated the accuracy of the global annual

TABLE 4. Estimation of Global Average OH

Interval Δt	Mass of CH_3CCl_3 in Atmosphere, kt	$\Delta CH_3CCl_3/\Delta t$, kt/year	Annual CH_3CCl_3 Emissions $\Delta E/\Delta t$, kt/year	Global Average OH $[OH]_g$, $\times 10^5$ cm^{-3}
Jan. – June 1980	2498	—	—	—
July – Dec. 1980	2507	155	552	8.5
Jan. – June 1981	2654	117	548	8.9
July – Dec. 1981	2687	133	548	8.4
Jan. – June 1982	2787	129	514	7.6
July – Dec. 1982	2817	111	514	7.8
Jan. – June 1983	2899	117	542	8.0
July – Dec. 1983	2935	—	—	—
Mean				8.2
SEM[a]				±0.2

[a] Standard error of the mean.

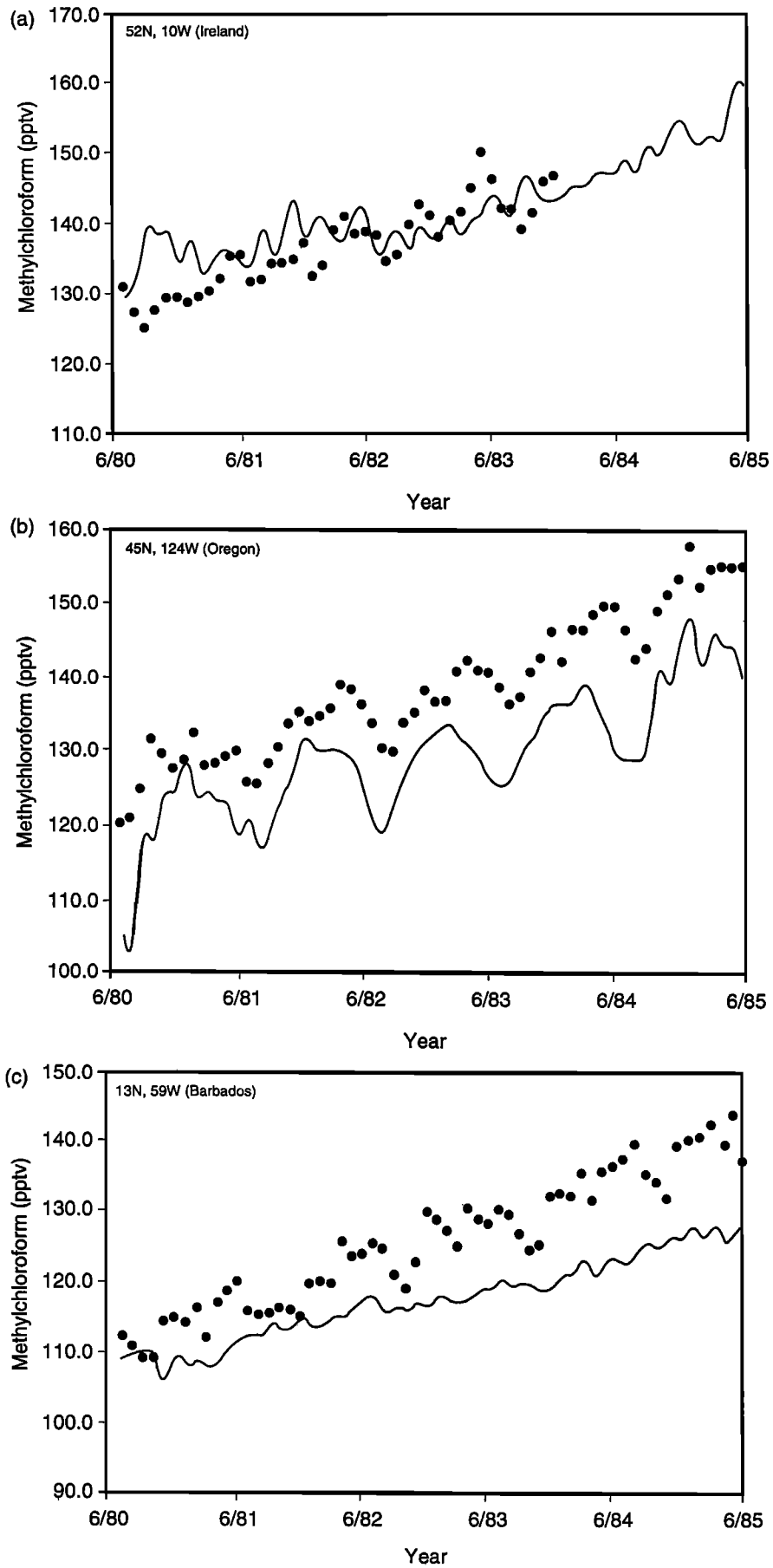

Fig. 7. Case 2. Modeled (solid line) and measured (dotted line) surface concentration of CH_3CCl_3 for the five ALE sites (*a*) Adrigole, Ireland, (*b*) Cape Meares, Oregon, (*c*) Ragged Point, Barbados, (*d*) American Samoa, and (*e*) Cape Grim, Tasmania.

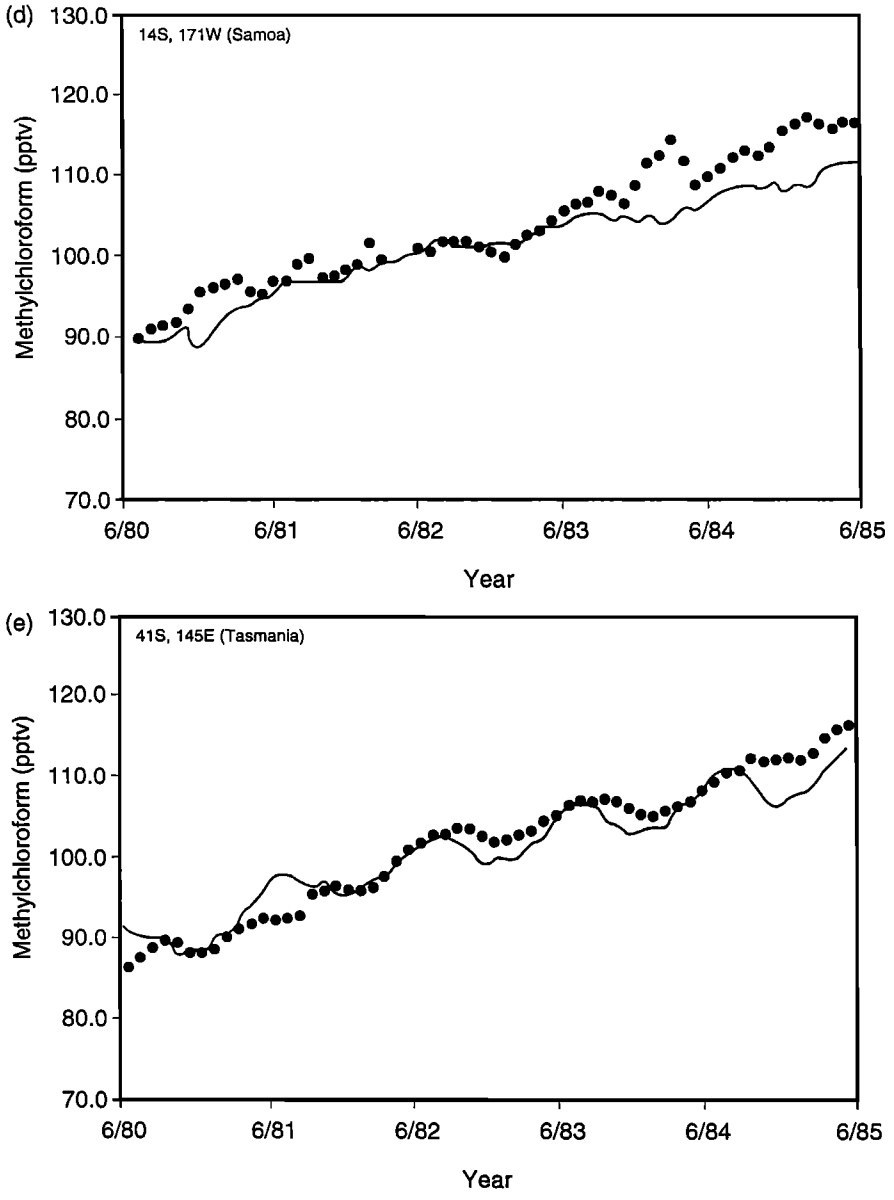

Fig. 7 (continued)

production term to be ±3%. The uncertainties associated with hemispheric emission rates, E_N and E_S, are unknown. Potentially significant uncertainties to E_N are associated with the absence of data on methyl chloroform production in China, Eastern Europe, and the former USSR.

We noted in case 2 that the existence of the ocean sink is implicitly included in the term $[CH_3CCl_3]_G$, which is experimentally determined by the ALE observations. Likewise, the terms $[CH_3CCl_3]_N$ and $[CH_3CCl_3]_S$ are determined from the ALE data record and thus implicitly include the effects of the ocean sink. This means that the value estimated for $[OH]_N/[OH]_S$ also captures the effects of the interhemispheric asymmetry of ocean surface area.

The value calculated for $[OH]_N/[OH]_S$ is 0.46, compared with 0.81 in case 2. We retained the same value for $[OH]_G$, $8.2 \times 10^5/cm^{-3}$. We scaled the monthly average OH values used in case 2 within each hemisphere accordingly. Figure 8 and Table 3 present the results of this simulation. The atmospheric lifetime for methyl chloroform remains unchanged, but the interhemispheric time constant decreased slightly to 5.7 months. The effect of decreasing the fraction of OH in the northern hemisphere was to improve the simulations for Oregon and Barbados but not for Ireland. The mean model bias for Oregon is now within the expected range (based on simulations of CFC-11 [*Kao et al.*, 1992]) of -5 to -8 ppt. In the southern hemisphere, where the average concentration of OH increased, the model biases at Samoa and Tasmania were not signifcantly affected. For all sites except Tasmania, the mean model biases are significant at the 95% confidence limit. The interhemispheric methyl chloroform gradient (Table 3*b*, column headed "N-S") is significantly improved compared to that in cases 1 and 2.

Case 4: Effect of an Ocean Sink for Methyl Chloroform

As noted earlier, recent observations indicate that CH_3CCl_3 is removed from the atmosphere at the ocean surface [*Butler et al.*, 1991]. They found the concentration of CH_3CCl_3 in the ocean surface waters to be nearly constant over large regions of the

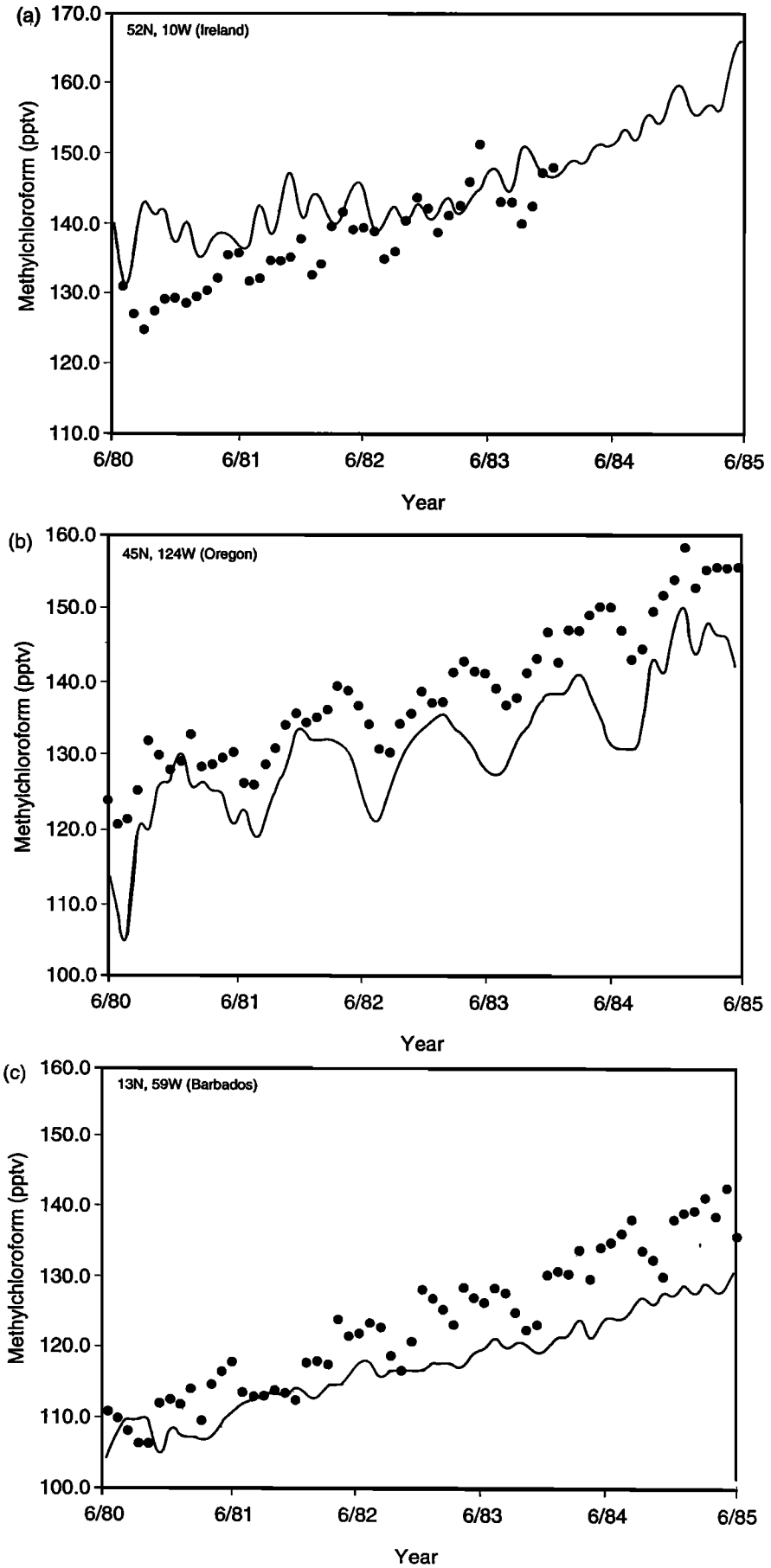

Fig. 8. Case 3. Modeled (solid line) and measured (dotted line) surface concentration of CH_3CCl_3 for the five ALE sites (*a*) Adrigole, Ireland, (*b*) Cape Meares, Oregon, (*c*) Ragged Point, Barbados, (*d*) American Samoa, and (*e*) Cape Grim, Tasmania.

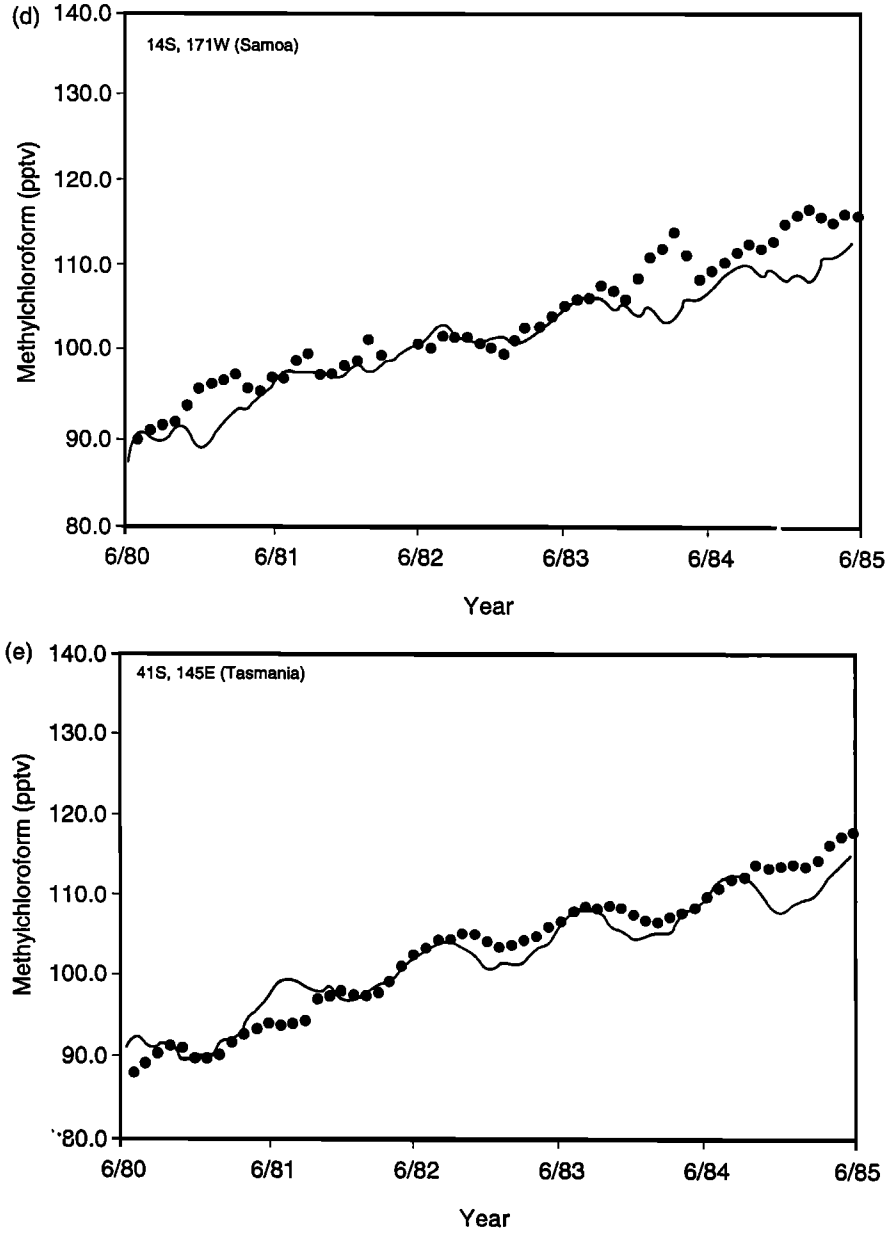

Fig. 8 (continued)

ocean. Extrapolating to the global ocean, they estimated that the total oceanic sink is ~5 to 11% of the global loss through reaction with OH.

The methodology employed in cases 2 and 3 for adjusting the $[OH]_G$ as well as $[OH]_N/[OH]_S$ implicitly incorporates this sink. We then tested how sensitive these empirical adjustments were to the existence of the ocean sink term. For this case, we elected to explicitly explore the effect of including an oceanic sink for methyl chloroform in the model. We set the ocean sink rate at 10% of the global loss rate of methyl chloroform by reaction with OH. We chose this value to explore the maximum effect suggested by *Butler et al.* [1991]. This sink is modeled as seasonally and spatially invariant with no dependence on wind speed.

This simulation is identical in all respects to that described as case 1 (c.f. Table 3*a*) with the addition of the sink for methyl chloroform at the ocean surface. Figure 9 and Table 3 present the results of the simulation. The atmospheric lifetime for methyl chloroform is reduced from 6.4 to 5.7 years, which is within acceptable bounds of 6.3 (+1.2, -0.9) years, and the interhemispheric transport time constant remains 6 months.

Model biases at the three northern hemisphere ALE sites were not significantly different than found for case 3. The model biases at Samoa and Tasmania changed sign from slightly negative in case 3 to slightly positive in case 4. The simulation of Samoa is quite good whereas that of Tasmania is somewhat degraded when compared with case 3. Thus the results of adjustments made to $[OH]_G$ and $[OH]_N/[OH]_S$ in cases 2 and 3 are, in general, closely matched by explicit inclusion of an ocean sink for methyl chloroform. However, note that the interhemispheric methyl chloroform gradient (Table 3*b*, column headed "N-S") returns to the same value as in cases 1 and 2. This suggests that, because of the small magnitude of the ocean sink, the interhemispheric difference in ocean surface area has less effect on the interhemispheric gradient of methyl chloroform than does the ratio $[OH]_N/[OH]_S$.

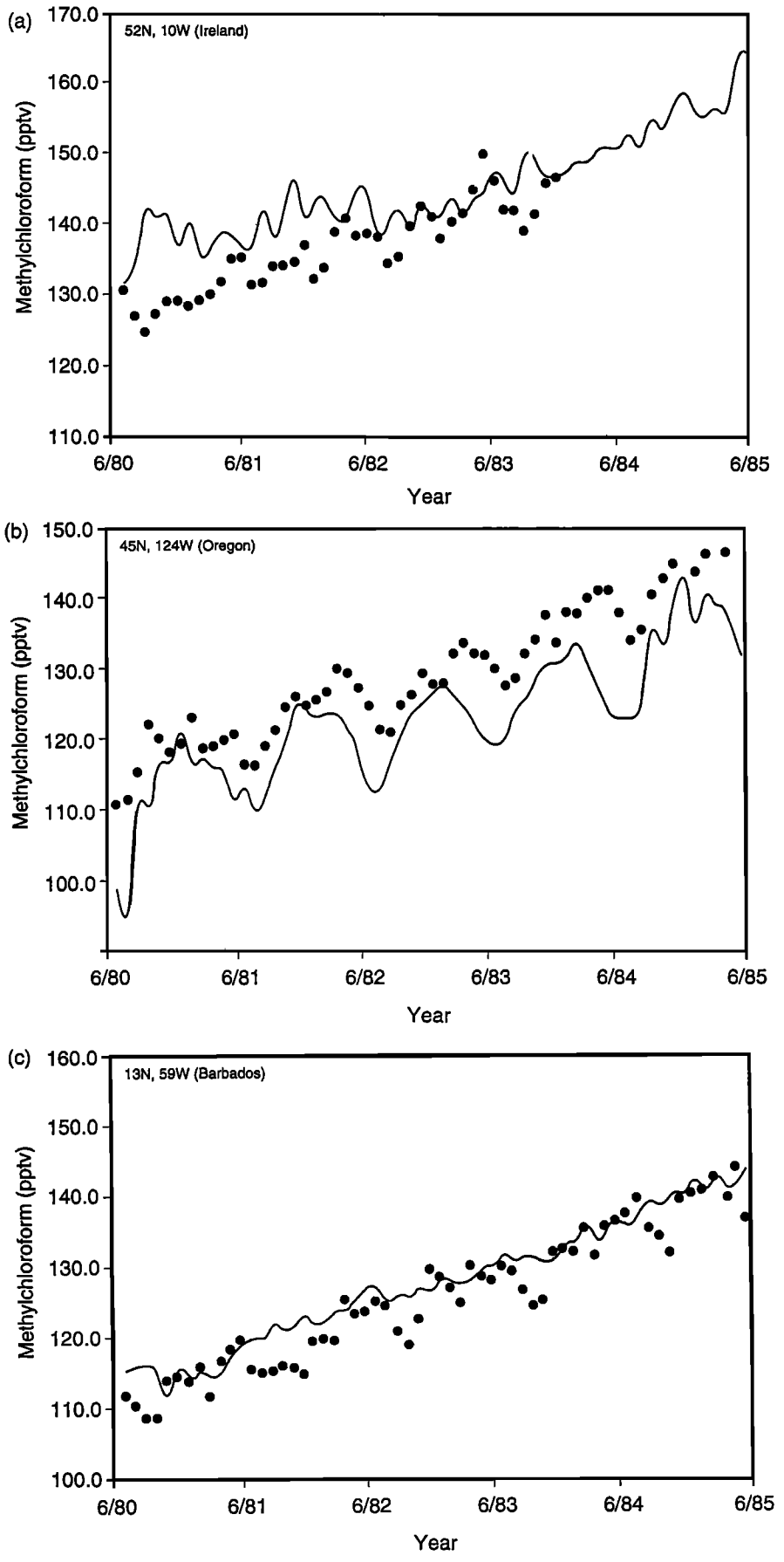

Fig. 9. Case 4. Modeled (solid line) and measured (dotted line) surface concentration of CH_3CCl_3 for the five ALE sites (*a*) Adrigole, Ireland, (*b*) Cape Meares, Oregon, (*c*) Ragged Point, Barbados, (*d*) American Samoa, and (*e*) Cape Grim, Tasmania.

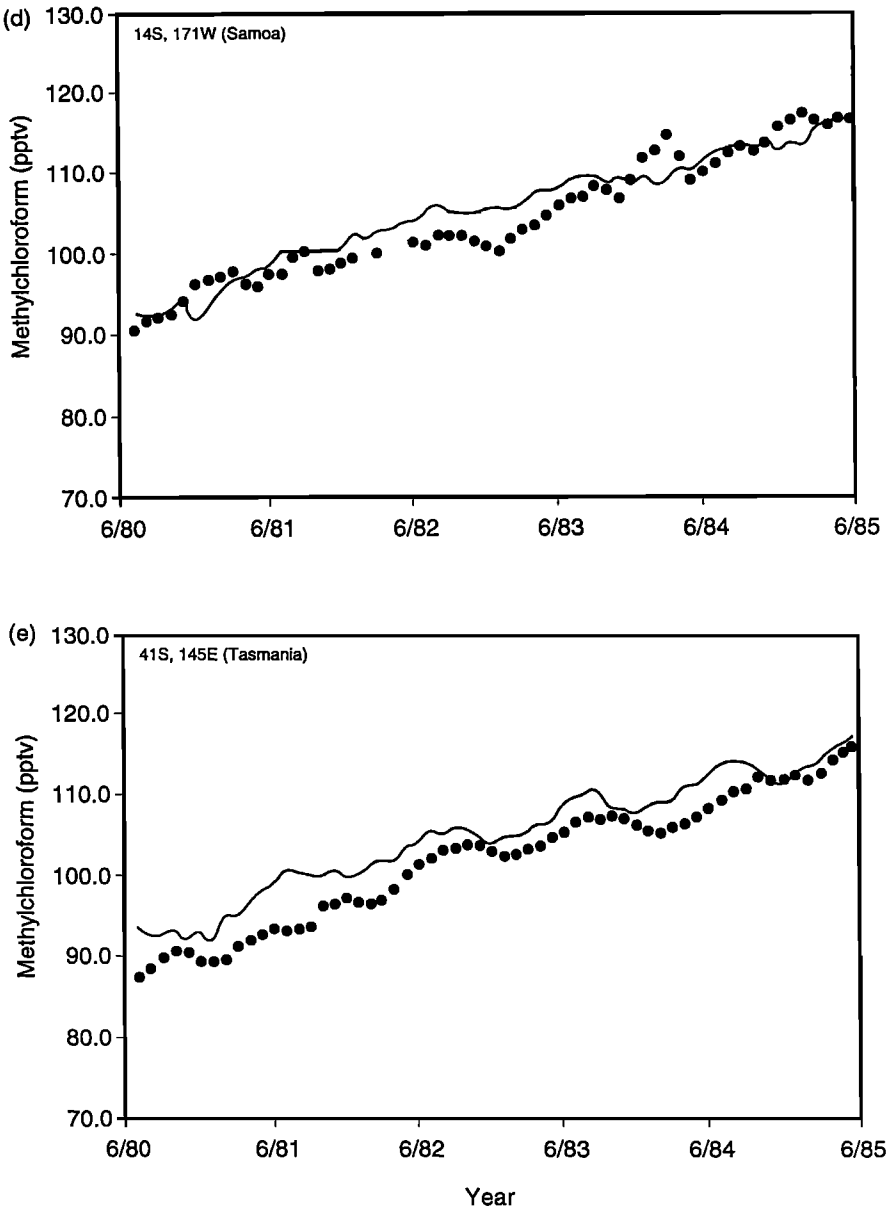

Fig. 9 (continued)

Summary of Findings from Cases 1 Through 4

Our best estimate of the annual average $[OH]_G$ is 6.5 ± 0.4 × 10^5 cm^{-3}. This value is within the uncertainty of the value found by *Prinn et al.* [1987] and very close to that of *Spivakovsky et al.* [1990] and *Taylor et al.* [1991]. Adjusting the global average ratio of $[OH]_N/[OH]_S$ from 0.81 to a value of 0.46, based on the observed interhemispheric gradient of methyl chloroform, improves the simulation of the global distribution and interhemispheric gradient of methyl chloroform. The improvement resulting from these adjustments is similar to that obtained by incorporating a 10% ocean sink for methyl chloroform. However, explicit inclusion of the ocean sink does not improve the simulation of the interhemispheric gradient of methyl chloroform, in spite of the interhemispheric difference in ocean surface area.

Significant differences have emerged from model studies of both tropospheric OH and the interhemispheric transport, based on the ALE methyl chloroform data, differences among inferred OH average values, and gradients of OH with latitude (see the recent exchange of comments and replies by *Hartley et al.* [1991] and *Cunnold et al.* [1991]). Of great interest is the disparity among research groups regarding the interhemispheric distribution of OH. The model of *Spivakovsky et al.* [1990] predicts a somewhat higher average concentration of OH in the northern than in the southern hemisphere. The model used by *Taylor et al.* [1991] and the one used in this study predict the opposite [*Tie et al.*, 1991].

Our results do not resolve all of these differences but, when taken with those of *Kao et al.* [1992], they further demonstrate that model transport characteristics may depend significantly on model structure. We have shown that it is possible to constrain (albeit somewhat imperfectly) the interhemispheric OH ratio from observations of the interhemispheric methyl chloroform gradient. As modeling of photochemical production of OH and interhemispheric transport improves and as the ALE data record lengthens with time, the method described here will aid refinement of the interhemispheric distribution of OH.

4. SEASONAL CYCLES OF CH_3Cl_3

We examined the annual cycle of CH_3CCl_3 in our model by using the simulation identified above as case 4, which includes the ocean sink for methyl chloroform. For each ALE site the seasonal cycle of methyl chloroform was calculated as described here. The interannual trends in the ALE observational record, the simulation, and model bias (the difference between the observation and the simulation) were removed by a least squares fit to a fourth-order polynomial. The 5-year mean and standard deviation of the monthly residuals for each of these variables at each ALE site are shown in Figure 10.

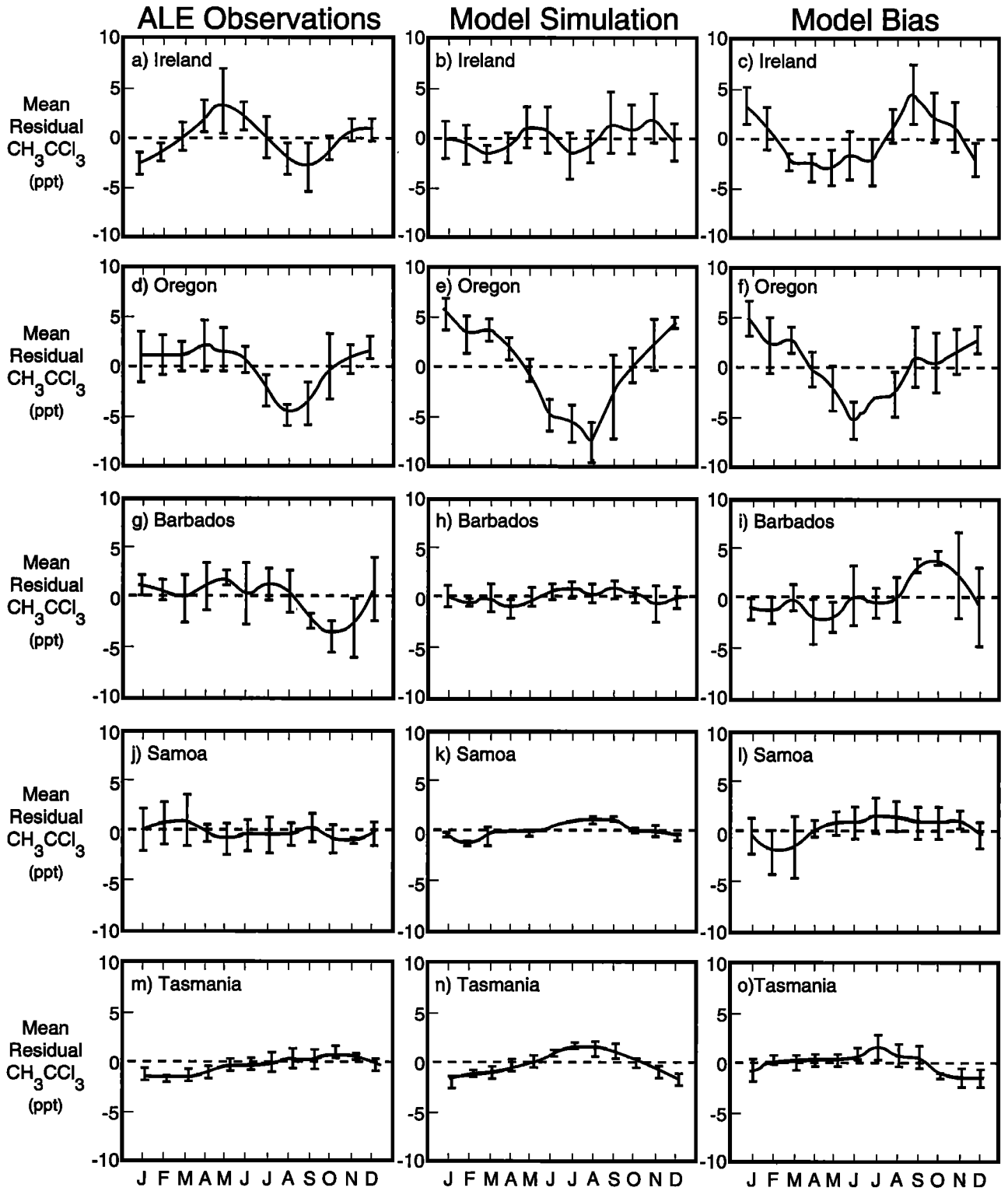

Fig. 10. The 5-year monthly mean residual concentration of methyl chloroform (parts per thousand). The observed seasonal cycle of CH_3CCl_3 (leftmost column), the modeled seasonal cycle (middle column), and model bias seasonal cycle (the difference between the modeled and observed cycles; rightmost column) are shown for (*a*) – (*c*) Adrigole, Ireland, (*d*) – (*f*) Cape Meares, Oregon, (*g*) – (*i*) Ragged Point, Barbados, (*j*) – (*l*) American Samoa, and (*m*) – (*o*) Cape Grim, Tasmania.

Ireland

For Ireland, the ALE observations (Figure 10*a*) exhibit a relative springtime maximum and autumn minimum that is not captured by the model (Figure 10*b*). The correlation between the observed and simulated seasonal cycles is poor (R = 0.05). The seasonal cycle of model bias (Figure 10*c*) reinforces this conclusion by showing that the differences between the curves in Figures 10*a* and 10*b* are significantly nonzero for most of the annual cycle. The seasonal cycle for the Ireland site is poorly simulated by the model because the model grid box containing Ireland includes major sources in western Europe. Furthermore, the model dynamics and chemistry that determine the seasonal cycle of the grid average residual methyl chloroform can differ significantly from the real atmospheric dynamics and chemistry affecting a single locale within that grid.

Oregon

For Oregon, the ALE observations exhibit a pronounced August minimum (Figure 10*d*). The model captures the seasonal cycle reasonably well (Figure 10*e*); the correlation coefficient is 0.77. The plot of the monthly model bias (Figure 10*f*) shows that, nevertheless, the phase and amplitude of the modeled seasonal cycle for the entire grid are significantly different from the observations at a single locale within the grid. As with Ireland, the model grid box containing Cape Meares includes major sources in the western United States. Likewise, grid-averaged model dynamics and chemistry can differ significantly from the regional scale dynamics and chemistry affecting a single locale within the grid.

Barbados

For Barbados (Figures 10*g* and 10*h*), the observations exhibit a minimum in the fall that is not captured by the simulation (R = -0.07). This feature is attributed to large-scale mixing of air with lower methyl chloroform concentrations from more southern latitudes during the hurricane season [*Hartley et al.*, 1991]. Tropical disturbances such as cyclones and hurricanes are not well simulated in this, nor any, GCM. Consequently, the seasonal cycle of model bias shows a pronounced overprediction in the fall (Figure 10*i*).

Samoa

For Samoa (Figures 10*j* and 10*k*), neither the ALE observations nor the simulation exhibit a strong seasonal cycle. However, the large variance in the residuals of the observations for December through March is a manifestation of significant interannual variability during these months. This has been attributed to the El Niño-Southern Oscillation [*Hartley et al.*, 1991]. This feature of the atmosphere is not captured by the GCM and, consequently, the correlation between the modeled and observed seasonal cycle is poor (R = -0.33). The model seasonal cycle (Figure 10*k*) exhibits a small minimum in the southern hemisphere summer and small maximum in the winter. The difference between these two curves (Figure 10*l*) is relatively featureless with no month exhibiting a statistically significant bias.

Tasmania

For Tasmania (Figure 10*m*), the ALE observations exhibit a weak seasonal cycle with a small maximum in October and minimum in February. The model exhibits a slightly different cycle with the maximum in July (Figure 10*n*). The correlation of the observed with the modeled seasonal cycle is moderately good (R = 0.54). The seasonal cycle of model bias shows significant departures from the observed seasonal cycle in winter and summer (Figure 10*o*). This feature hints that the amplitude of the seasonal cycle of OH in the southern hemisphere may be somewhat too large.

Effect of the Ocean Sink for Methyl Chloroform

The incorporation of a seasonally invariant and spatially constant ocean sink into the model does not significantly alter the calculated seasonal cycle of methyl chloroform. We compared the modeled seasonal cycles at the ALE locations for cases 1 and 3 (without and with the ocean sink for methyl chloroform, respectively) and found no statistically significant difference between these two cases. The measurements of ocean sink for methyl chloroform showed no dependence on sea surface temperature [*Butler et al.*, 1991]. However, Butler et al. note that the temperature range sampled may not have been large enough to discern an effect. They also noted several other physical processes that may influence the flux of methyl chloroform from the atmosphere to the ocean. If any of these processes are seasonally dependent, they may affect the seasonal cycle of methyl chloroform over the oceans.

Role of Chemistry Versus Transport in the Simulated Seasonal Cycle of Methyl Chloroform

Comparison of the modeled seasonal cycle of CFC-11 and CH_3CCl_3 separates the effects of model transport versus model OH on the seasonal cycles of CH_3CCl_3. We use the correlation coefficient (R) between the simulated monthly average CH_3CCl_3 and CFC-11 seasonal cycles to examine the relative importance of atmospheric transport versus atmospheric chemistry in influencing the seasonal cycle of CH_3CCl_3. If CH_3CCl_3 were not destroyed by reaction with OH, the value of R would be unity at all locations because the model source distribution and transport are identical to those used for simulating CFC-11. Departures from unity are a measure of the influence of the OH seasonal cycle on the CH_3CCl_3 seasonal cycle. Figure 11 shows the correlation between the seasonal cycles of CH_3CCl_3 and CFC-11 in 4.5° latitude bands at the surface. In the northern hemisphere, the average value of R is 0.75. This indicates that the modeled seasonal cycle of CH_3CCl_3 in the northern hemisphere is strongly influenced by atmospheric transport. The value of R declines across the equator to an average value of 0.1 in the southern hemisphere. We interpret this as evidence that the seasonal cycle of methyl chloroform is weakly influenced by model transport and is, consequently, more strongly influenced by the phase and amplitude of the modeled seasonal cycle of OH.

5. SUMMARY OF FINDINGS

This model of the global distribution of CH_3CCl_3 simulates the 5-year record of observations made at the five ALE sampling sites, generally to within 5% of the observed annual mean concentration. The calculated average global lifetime, 5.7 ± 0.3 years, is within the range [6.3 (+1.2, -0.9) years] estimated from ALE measurements [*Prinn et al.*, 1987]. The estimated global mean OH concentration is $6.5 \pm 0.4 \times 10^5/cm^{-3}$. The reaction rate between OH and methyl chloroform has recently been remeasured and revised downward from the value used in this study [*Talkudar et al.*, 1992]. The effect of this revision is to increase

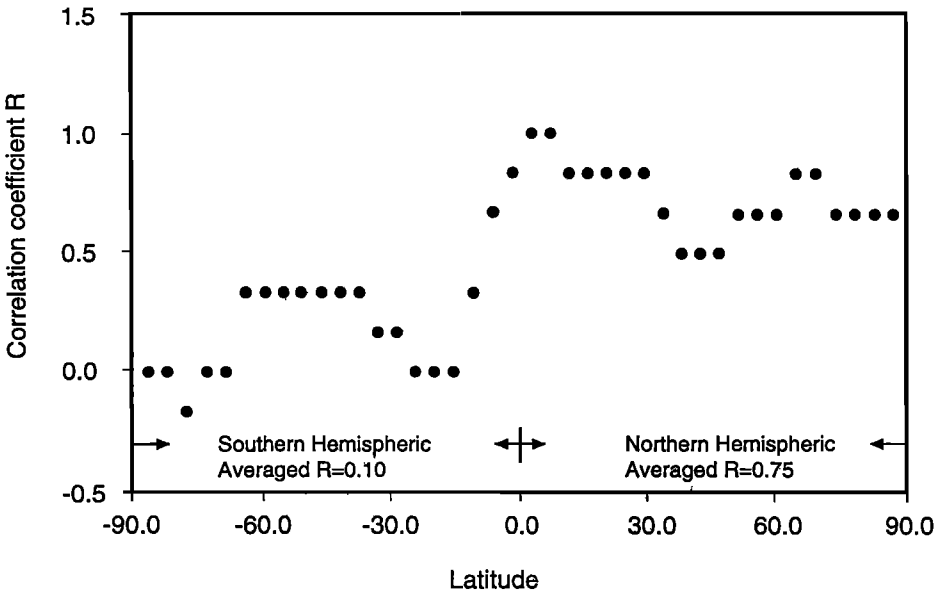

Fig. 11. Latitudinal distribution of the correlation coefficient (R) between the seasonal cycle of CFC-11 and the seasonal cycle of CH_3CCl_3 from 1980 to 1985.

our estimated global mean OH concentration by ~15%. The effect of this change on the interhemispheric gradient of methyl chloroform is being investigated.

Empirical adjustment of the annual average $[OH]_G$ and $[OH]_N/[OH]_S$ as calculated by a simple two-dimensional photochemical model significantly improves the simulated global distribution of methyl chloroform. The improvement is similar to that obtained by incorporating a 10% ocean sink for methyl chloroform. However, inclusion of the ocean sink does not improve the simulation of the interhemispheric gradient of methyl chloroform, in spite of the interhemispheric difference in ocean surface area. A larger oceanic sink than we have considered here—or one with large spatial or seasonal variations—could alter our results. This possibility should be investigated further through oceanic measurements and future modeling.

The model confirms that CH_3CCl_3 predominantly released at the surface in the northern hemisphere is quickly mixed throughout the northern troposphere. Transport to the southern hemisphere occurs preferentially between 600 and 300 mbar as part of the Hadley cell circulation. The interhemispheric time constant is ~6 months with ~270 kt/year being transported from the northern to southern hemisphere. But these values are sensitive to the interhemispheric gradient of OH.

The seasonal cycles of methyl chloroform measured at the ALE sites are not fully captured by the model. Some of the reasons for the model's inability to accurately simulate the seasonal cycle include variability in the observations due to phenomena such as regional scale (i.e., subgrid) circulation patterns, tropical storms, and El Niño-southern-oscillation events that are not simulated by the parent GCM. Our two-dimensional model of the distribution of OH is deficient in its treatment of nonmethane hydrocarbons. The assumed spatial and temporal constancy of the ocean sink for methyl chloroform has not been confirmed by observations.

In the northern hemisphere, the seasonal cycles of CH_3CCl_3 in the model are mainly controlled by the effects of atmospheric dynamics in transporting CH_3CCl_3 from the source regions to the sampling locations. However, in the southern hemisphere, the modeled seasonal cycles of CH_3CCl_3 are more strongly influenced by the amplitude of the seasonal cycle of OH.

Three-dimensional simulations of the global biogeodynamics of atmospheric methane, nonmethane hydrocarbons, and other trace gases depend on an accurate representation of the global OH field. Models of this type, from which the OH distribution can be inferred, will continue to be necessary until experimental methods are developed that can map the global distribution of OH and monitor the seasonal concentration changes and annual trends.

Acknowledgments. We thank C. F. Keller Jr. and S. Barr of Los Alamos National Laboratory for their suggestions and support for this study. We appreciate the efforts of R. Malone and G. Glatzmaier, who have made several improvements to the Los Alamos GCM. R.J.C. acknowledges support from NASA contract W-16,184. This research project was funded by the United States Department of Energy and the University of California INCOR program.

REFERENCES

Brasseur, G., M. H. Hitchman, S. Walters, M. Dymek, E. Falise and M. Pirre, An interactive chemical dynamical radiative two-dimensional model of the middle atmosphere, *J. Geophys. Res.*, *95*, 5639-5655, 1990.

Brune, W. H., Stalking the elusive atmospheric hydroxyl radical, *Science*, *256*, 1154-1155, 1992.

Butler, J. H., W. Elkins, T. M. Thompson, B. D. Hall, T. H. Swanson and V. Koropalov, Oceanic consumption of CH_3CCl_3: Implications for tropospheric OH, *J. Geophys. Res.*, *96*, 22,347-22,355, 1991.

Chameides, W. L. and A. Tan, The two-dimensional diagnostic model for tropospheric OH: An uncertainty analysis, *J. Geophys. Res.*, *86*, 5209-5223, 1981.

Cunnold, D. M., R. G. Prinn and C. M. Spivakovsky, Comment and Reply on Tropospheric OH in a three-dimensional chemical tracer model: An assessment based on observations of CH_3CCl_3, *J. Geophys. Res.*, *96*, 17391-17398, 1991.

DeMore, W. B., R. F. Hampson, D. M. Golden, C. J. Howard and M. J. Molina, Chemical kinetics and photochemical data for use in stratospheric modeling, Pub. 90-1, Jet Propulsion Lab., Pasadena, Calif., 1990.

Fraser, P. J., P. Hyson, R. A. Rasmussen, A. J. Crawford and M. A. K. Khalil, Methane, carbon monoxide and methyl chloroform in the Southern Hemisphere, *J. Atmos. Chem.*, *4*, 3-42, 1986.

Hartley, D., et al., Comment and Reply on Tropospheric OH in a three-dimensional chemical tracer model: an assessment based on observations of CH_3CCl_3, *J. Geophys. Res.*, *96*, 17,383-17,390, 1991.

Houghton, J. T., G. J. Jenkins and J. J. Ephraums (Eds.), *Climate Change:*

The IPCC Scientific Assessment , Cambridge University Press, New York, 1990.

Kao, C.-Y., X. Tie, E. J. Mroz, F. N. Alyea and D. M. Cunnold, Simulation of the global CFC-11 using the Los Alamos chemical tracer model, *J. Geophys. Res.*, *97*, 15,827-15,838, 1992.

Khalil, M. A. K. and R. A. Rasmussen, The atmospheric lifetime of methyl chloroform, *Tellus*, *36 Sec.B*, 317-332, 1984.

Knapska, D., U. Schmidt, C. Jebsen, G. Kulessa, J. Rudolph and S. A. Penkett, Vertical profiles of chlorinated source gases in the mid-latitude stratosphere, in *Atmospheric Ozone*, edited by C. S. Zerefos and A. Ghazi, D. Reidel, Dordrecht, 1985, pp. 117-121.

Lovelock, J. E., Methyl chloroform in the troposphere as an indicator of OH radical abundance, *Nature*, *32*, 267, 1977.

Malone, R. C., L. H. Auer, G. A. Glatzmaier, M. C. Wood and O. B. Toon, Nuclear winter: Three-dimensional simulations including interactive transport, scavenging, and solar heating of smoke, *J. Geophys. Res.*, *91*, 1039-1056, 1986.

Midgley, P. M., The production and release to the atmosphere of 1,1,1-trichloroethane (methyl chloroform), *Atmos. Environ.*, *23*, 2663-2665, 1989.

Prather, M., M. B. McElroy, S. Wofsy, G. Russell and D. Rind, Chemistry of the global troposphere: Fluorocarbons as tracers of air motion, *J. Geophys. Res.*, *92*, 6579-6613, 1987.

Prinn, R. G., F. N. Alyea and D. M. Cunnold, Stratospheric distributions of odd nitrogen and odd hydrogen in a two-dimensional model, *J. Geophys. Res.*, *80*, 4997-5004, 1975.

Prinn, R. G., *et al.*, Atmospheric trends in methyl chloroform and the global average for the hydroxyl radical, *Science*, *238*, 945-950, 1987.

Ramanathan, V., et al., Climate-chemical interactions and effects of changing atmospheric trace gases, *Rev. Geophys.*, *25*, 1441-1482, 1987.

Rasmussen, R. A. and M. A. K. Khalil, Atmospheric fluorocarbons and methyl chloroform at the South Pole, 1982, *Antarct. J. U.S.*, *17*, 203-205, 1983.

Rasmussen, R. A., M. A. K. Khalil and J. S. Chang, Atmospheric trace gases over China, *Environ. Sci. Technol.*, *16*, 124-126, 1982.

Spivakovsky, C. M., R. Yevich, J. A. Logan, S. C. Wofsy, M. B. McElroy and M. J. Prather, Tropospheric OH in a three-dimensional chemical tracer model: An assessment based on observations of CH_3CCl_3, *J. Geophys. Res.*, *95*, 18,441-18,471, 1990.

Talkudar, R. K., A. Mellouki, A.-M. Schmoltner, T. Watson, S. Montzka and A. R. Ravishankara, Kinetics of the OH reaction with methyl chloroform and its atmospheric implications, *Science*, *257*, 227-230, 1992.

Taylor, J. A., G. P. Brasseur, P. R. Zimmerman and R. J. Cicerone, A study of the sources and sinks of methane and methyl chloroform using a global 3-D Lagrangian tropospheric tracer transport model, *J. Geophys. Res.*, *96*, 3013-3044, 1991.

Tie, X., F. N. Alyea, D. M. Cunnold and C.-Y. J. Kao, Atmospheric methane: A global three-dimensional model study, *J. Geophys. Res.*, *96*, 17,339-17,348, 1991.

F. N. Alyea, and D. M. Cunnold, School of Earth and Atmospheric Sciences, Georgia Institute of Technology, Atlanta, GA 30332-0340.

R. J. Cicerone, Dept. of Geosciences, University of California at Irvine, Irvine, CA 92717.

C.-Y. Kao and E. J. Mroz, MS J514, Los Alamos National Laboratory, Los Alamos, NM 87544.

X. Tie, Scripps Institution of Oceanography, University of California at San Diego, La Jolla, CA 92093.

(Received July 22, 1991;
revised August 21, 1992;
accepted August 31, 1992.)